Field localization and enhancement near the Dirac point of a finite defectless photonic crystal

Giuseppe D'Aguanno,[1,*] Nadia Mattiucci,[1] Claudio Conti,[2] and Mark J. Bloemer[3]
[1]*AEgis Tech., Nanogenesis Division 410 Jan Davis Dr, Huntsville, Alabama 35806, USA*
[2]*Department of Physics, University Sapienza, Piazzale A. Moro 2, 00185 Rome, Italy*
[3]*Charles M. Bowden Laboratory, Army Aviation and Missile Research, Development, and Engineering Center, Redstone Arsenal, Alabama 35898, USA*
(Received 11 October 2012; published 26 February 2013)

We use a rigorous electromagnetic approach to show the existence of strongly localized modes in the stop band of a linear, two-dimensional, finite photonic crystal near its Dirac point. At normal incidence, the crystal exhibits a Dirac point with 100% transmission. At angles slightly off the normal, where the crystal is 100% reflective, instead of exponentially decaying fields as in a photonic stop band, the field becomes strongly localized and enhanced inside the crystal. We explain that this anomalous localization is due to guided mode resonances that are the foundation of the Dirac point itself and also shape its adjacent band gap. Besides shedding new light on the physical origin of Dirac points in finite photonic crystals, our results could have applications in many nonlinear light-matter interaction phenomena in which it is crucial to achieve a high degree of light localization.

DOI: 10.1103/PhysRevB.87.085135 PACS number(s): 42.70.Qs, 42.25.Bs, 42.25.Gy

I. INTRODUCTION

In the last few years there has been increasing interest in the study of Dirac points in two-dimensional photonic crystals;[1–7] i.e., points where two photonic bands touch as a pair of cones (Dirac cones) giving rise to a linear, instead of a parabolic, dispersion for photons. Dirac cones and Dirac points owe their names to the formal analogy existing between the two-dimensional Helmholtz equation describing the electromagnetic behavior of photons near these points and the Dirac equation for the motion of relativistic, free electrons in the absence of external fields. The subject is well-rooted in solid state physics, in which Dirac cones appear in a great variety of scenarios such as non-relativistic motion of particles in a crystal[8] and semiconductor nanostructures for spintronic applications.[9] Particularly important in this framework is the recent discovery of graphene,[10] a purely two-dimensional electronic system in which the conduction band and the valence band touch each other at the Dirac point, leading to remarkable electronic transport properties.[11] In the electromagnetic domain, photonic crystals exhibiting Dirac cones have been studied, for example, in the context of conical diffraction.[12] Moreover, in some recent publications, photonic crystals exhibiting Dirac cones have been shown to have analogies with vacuum impedance-matched, zero-refractive index metamaterials.[6,7,13] Conventional zero-refractive index metamaterials generally rely on metallic structures, metallic inclusions, or both,[14] whose inherent losses may actually hamper and/or reduce the functionality of any proposed device, especially in the visible range. In the photonic crystal case, the structures can be made entirely of dielectric or semiconductor materials, or both, with evident benefits in terms of loss reduction.

In this work we show another important property of light near the Dirac point of a two-dimensional, finite, defectless photonic crystal; i.e., the existence of strongly localized modes in its neighboring stop band. Our approach relies on a full numerical simulation of Maxwell equations, which we carry out by using an in-house–developed numerical code based on the Fourier modal method (FMM).[15]

II. RESULTS AND DISCUSSION

We start by describing in Fig. 1(a) a two-dimensional, finite photonic crystal made of a square lattice of dielectric columns.

The incident field is considered to be a plane, monochromatic, electromagnetic wave of frequency ω with the electric vector polarized along the axis of the columns (TE polarization). For $r/a = 0.2$ and $\varepsilon = 12.5$, this structure is known to possess a Dirac point at $\omega a/2\pi c \cong 0.54$ for normal incidence at the Γ point as in Ref. 6. In Fig. 1(b) we show the transmittance of a five-period photonic crystal as a function of incident angle and frequency. The transmittance illustrates the typical "band structure" associated with a Dirac point: two passbands that touch each other in one point surrounded by a stopband (although, here, we plot the incident angle instead of the wave vector). In Fig. 2 we show the transmittance vs frequency at normal incidence and several incident angles close to the normal. We note that at normal incidence, the photonic crystal acts as a perfect transparent material. As the incident angle moves away from normal incidence, a stopband opens in the form of a transmission anti-resonance (or reflection resonance), whose spectral bandwidth widens with increasing incident angles. This behavior is in agreement with the overall characteristics of the transmission band structure shown in Fig. 1(b).

In Fig. 3, we show the field localization properties. In particular, in Fig 3(a) the field is calculated at the frequency corresponding to the Dirac point where total transmission is achieved ($T = 1$), whereas in Fig 3(b), the field is calculated at the frequency of the transmission minimum ($T < 0.001\%$) of the stopbands corresponding to $\vartheta = 0.1^\circ$.

In Fig. 3(a), each of the five rows of columns of the structure shows exactly the same field localization properties, in agreement with the fact that at the Dirac point, the photonic crystal becomes perfectly transparent, as expected for a vacuum-impedance-matched metamaterial.[6,7,13] In this case the transmission mechanism is based on an effective impedance matching: the wave does not experience any change in effective impedance, and it can propagate through the structure with nearly uniform amplitude, no amplification,

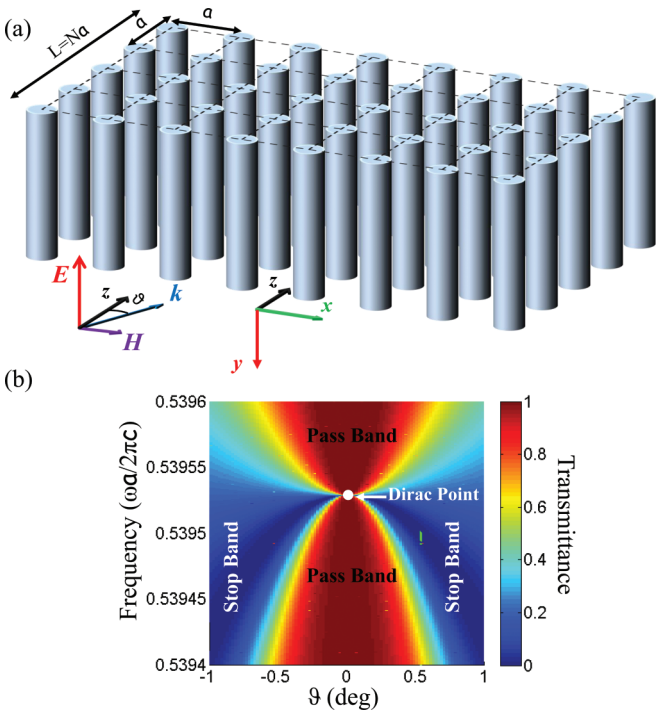

FIG. 1. (Color online) (a) A two-dimensional photonic crystal made of a square lattice (lattice constant a) of dielectric columns with radius r and electric permittivity ε. The photonic crystal is five periods long in the z direction with length $L = N$a, where N is the number of rows of columns. A plane electromagnetic wave with the electric field parallel to the axis of the cylinders is incident on the structure with its k-vector in the (x, z) plane (in-plane coupling), forming an angle ϑ with respect to the z direction. (b) Transmittance in the (ω, ϑ) plane around the Dirac point numerically calculated by the FMM. The structure's parameters are $N = 5$, r/a $= 0.2$, $\varepsilon = 12.5$.

and minimum reflections (see also Fig. 3(c) for a section of the field localization profile over the structure). On the other hand, in Fig. 3(b) at the transmission minimum of the stopband corresponding to $\vartheta = 0.1^\circ$, we find quite surprisingly that the field intensity is strongly localized in the central row with the maximum intensity reaching an astounding $\sim 10^4$. A section of the field localization profile for the two cases is shown in Fig. 3(c). Note in Fig. 3(c) that the envelope of the field profile at the transmission minimum has a bell shape. This

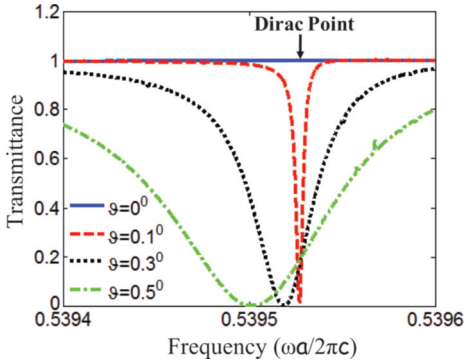

FIG. 2. (Color online) Transmittance vs frequency for different incident angles.

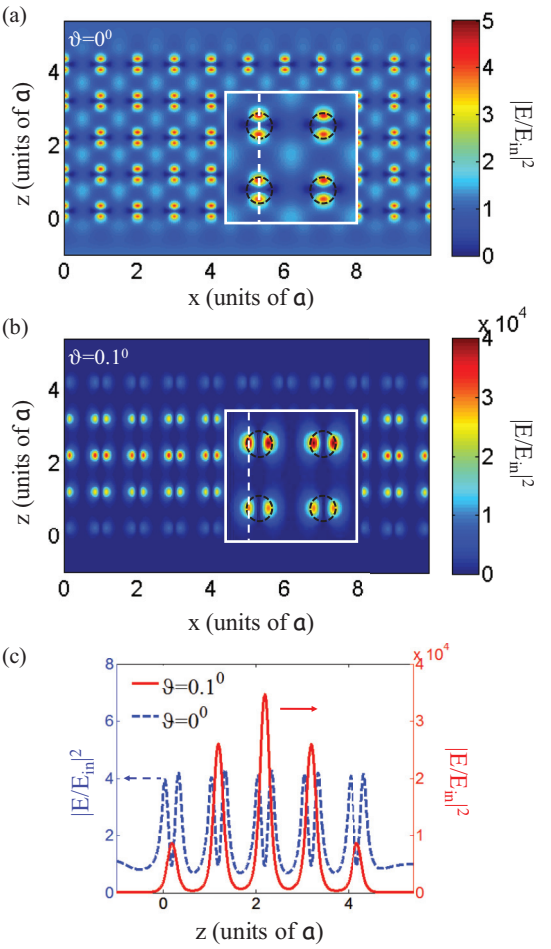

FIG. 3. (Color online) (a) Cross-sectional view of the electric field intensity normalized to the incident field intensity at the Dirac point where $T = 1$. (b) Cross-sectional view of the field localization in the stopband at the transmission minimum for $\vartheta = 0.1^\circ$. The insets show a magnification of the field localization on the columns. The dashed circles indicate the position of the columns. The dashed line parallel to the z axis indicates the section of the field that it is shown in Fig. 3(c). (c) Section of the field intensity profiles along the z axis for the two cases.

is in stark contrast to a photonic crystal stopband, in which the envelope decays exponentially from the incident interface. The bell-shaped envelope and the large field enhancement at the Dirac stopband are more typical of a photonic band edge that has unity transmission.

Field localizations similar to that of the $\vartheta = 0.1^\circ$ case are also found for larger angles up to approximately 1°, although for these larger angles the peak intensity decreases and the spectral bandwidth of the associated transmission anti-resonance widens. By defining an anti-resonance quality factor as $Q_{ar} = \omega_c / \Delta\omega$, where, in analogy with the quality factor for resonances in a conventional cavity, $\Delta\omega$ is the full-width half maximum, whereas in our case, ω_c is the anti-peak frequency, the average electromagnetic energy density stored in the structure scales as Q_{ar}.

We have also calculated the participation ratio (PR) and localization length (ξ) with the following standard equations:[16] $PR = \iint |E(x,z)|^4 dxdz / (\iint |E(x,z)|^2 dxdz)^2$, $\xi = 1/\sqrt{PR}$.

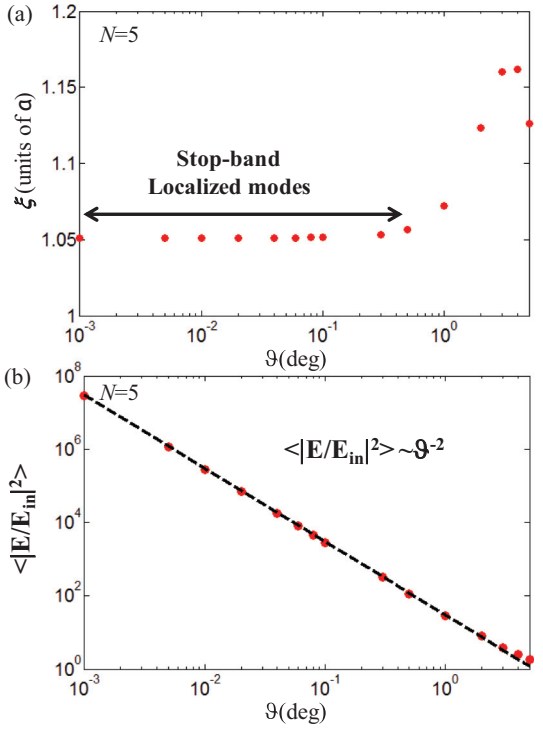

FIG. 4. (Color online) (a) Localization length vs incident angle for the $N = 5$ period structure. (b) Average field localization vs incident angle. In the Supplemental Materials (StopBandModes.wmv),[17] we show the field localization for the different angles and the transition from localized to evanescent modes.

Along x the integral is performed over the elementary cell. In Fig. 4(a) we show ξ and in Fig. 4(b) the average field intensity, both as function of the incident angle. For each angle, the quantities have been calculated at the frequency of the respective reflection resonances.

In Fig. 4(a) it is noted that ξ remains practically constant until $\vartheta \sim 1^\circ$, when it starts to increase. This increase in the localization length marks the transition of the stopband modes from localized to evanescent. The corresponding field localization for the different angles is shown in the Supplemental Material.[17] The average field localization shown in Fig. 4(b) scales exactly as ϑ^{-2}, in agreement with the previously explained decrement of the quality factor of the respective transmission anti-resonances as the incident angle increases. The average field localization starts to depart from the ϑ^{-2} law as the stopband modes transition from localized to evanescent. The average field intensity reaches values close to 10^8 for incident angles near 0.001°. It is quite remarkable to achieve such a strong field confinement in a photonic crystal that is only five periods long. Additional calculations have also been performed (Fig. 5) by increasing the number of periods of the structure from $N = 3$ to $N = 15$ for a fixed incident angle at $\vartheta = 0.1^\circ$. We find in this case that the localization length scales as $N^{0.46}$, and the average field localization scales as $1/N^2$. Note that even in the case of $N = 15$ the field is still well localized in the bulk of the structure with a bell-shaped envelope.

To shed some light on the nature of the field localization, in Fig. 6 we have compared side by side the transmittance of the structure and the coupling strength (CS) of the leaky

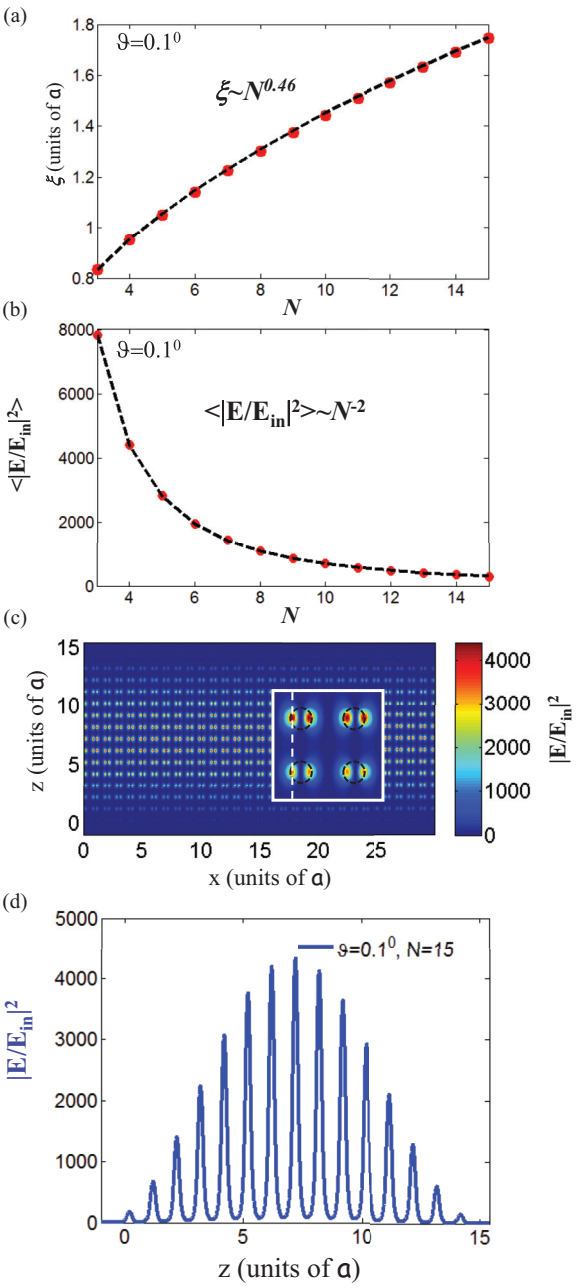

FIG. 5. (Color online) (a) Localization length and (b) average field localization compared with number of periods for $\vartheta = 0.1^\circ$. (c) Cross-sectional view of the field localization in the stopband at the transmission minimum for $\vartheta = 0.1^\circ$ and $N = 15$. The inset shows a magnification of the field localization on the columns. The dashed circles indicate the position of the columns. The dashed line parallel to the z axis indicates the section of the field that it is shown in Fig. 5(d). (d) Section of the field intensity profile along the z axis.

waveguide modes propagating along the x axis of the photonic crystal. In general, for any non-absorbing, planar structure subject to transverse momentum conservation k_x, the poles of the transmission of the electric field lie over the real k_x axis and are associated with the guided modes supported by the structure.[18] In our case, the photonic crystal is not "*sensu stricto*" a waveguide, but still supports leaky modes that can be excited by the incident field thanks to the additional

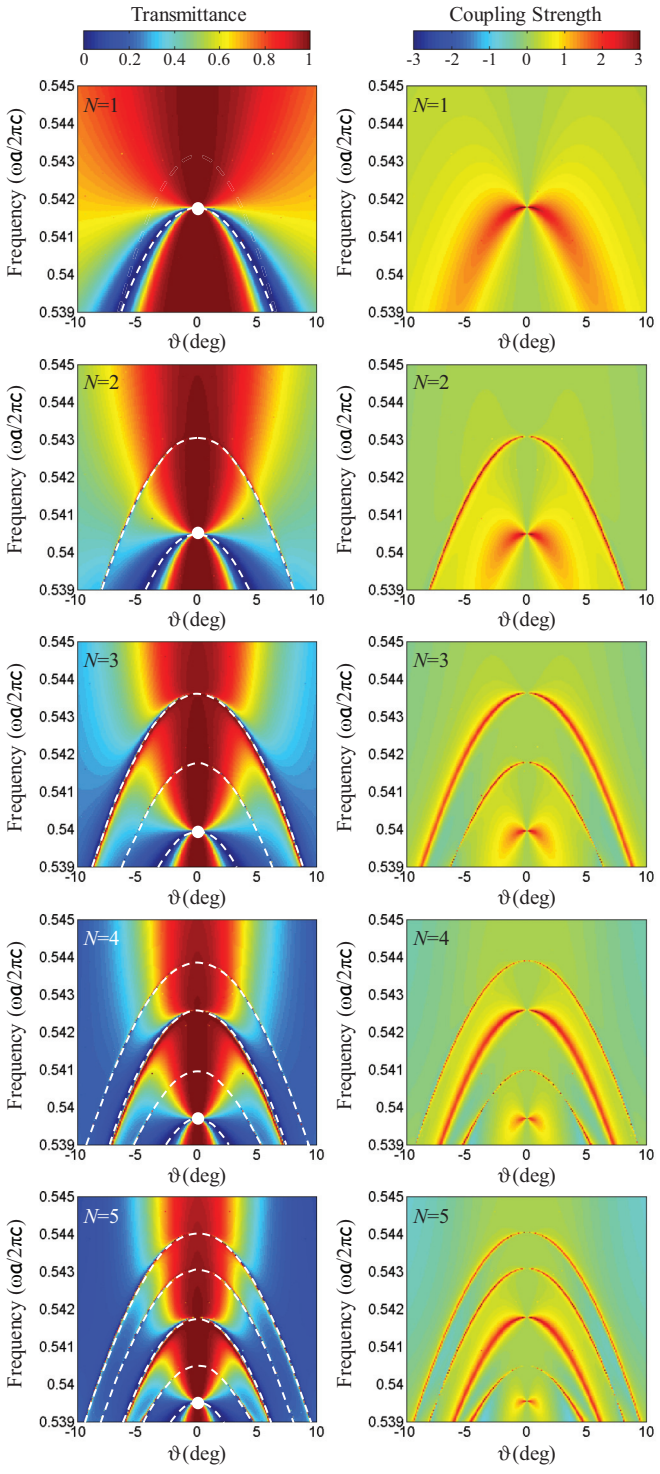

FIG. 6. (Color online) Transmittance and coupling strength in the (ω, ϑ) plane for different periods. The white dot indicates the position of the Dirac point. The dashed lines represent the dispersion of the GMRs.

momentum provided by the periodicity of the structure. These modes are usually called guided mode resonances (GMRs), and they generally appear in the form of Fano resonances.[19] In this case the poles of the transmission migrate into the complex plane; nevertheless, the maxima of the transmission along the real axis describe quite accurately the dispersion of those leaky modes. The coupling strength has been calculated as $CS = \log_{10}(\sum_m |t_m|^2)$, where t_m is the electric field transmission coefficient of the mth diffracted order. We have started by studying just a single row of columns and proceeded up to $N = 5$. In the figures, the dashed lines represent the dispersion of the GMRs. The $N = 1$ case is very instructive because it clearly shows the crucial role played by the GMRs in the formation of the Dirac point and its related anomalous localization properties. The figure shows that even in the $N = 1$ case a Dirac point is created whose position is determined by the corresponding GMR of the structure. This GMR also shapes the neighboring stopband, as can be observed by looking at the coupling strength. The coupling of this GMR increases as ϑ approaches zero but is strictly forbidden at the Dirac point where $\vartheta = 0^\circ$. As the angle increases beyond 1°, the GMR intersecting the Dirac point degenerates into a classical stopband evanescent mode.

Adding more periods does not change the basic mechanism just described. The position of the Dirac point and its neighboring stopband are shaped by the corresponding GMR, which we call the Dirac-point GMR. The decrement of the coupling strength of the Dirac-point GMR as the incident angle departs from the near-to-normal condition is quite peculiar. Conventional GMRs, in both dielectric and plasmonic structures, are dispersive and generally maintain their coupling strength for a wide range of incident angles.[20] It is indeed possible even in our case to ascertain, by looking at the coupling strength, that all other GMRs except for the Dirac-point GMR, are robust at large angles of incidence.

The different characteristics of a field tuned at the Dirac point and at the GMR near the Dirac point are shown in a second animation in the Supplemental Material,[21] where the electric field temporal evolution is shown at $\vartheta = 0^\circ$ and at $\vartheta = 1^\circ$ for the $N = 5$ period case. In the animation, the central rectangle in each 0° and 1° field movie is an x-zoom of a single x-period to observe the temporal evolution of the field localization over the columns.

At the Dirac point the photonic crystal basically acts as perfect transparent material; the wave- front of the incident field undergoes minimal distortion as it propagates through the crystal, and it is completely transmitted. On the contrary, at the GMR near the Dirac point, the field is coupled into the structure along the x axis (i.e., in the transverse direction with respect to the incident), with strong localization in the interior of the structure, and then completely reflected.

To demonstrate the generality of these modes, we also show in Fig. 7 a second example of a finite photonic crystal. In this latter case, the columns are arranged in a triangular lattice with $r/a = 0.3$ and $\varepsilon = 11.4$, and the incident wave has the H-field parallel to the axis of the columns (transverse magnetic [TM] polarization). The structure is known to possess a Dirac point at $\omega a/2\pi c \cong 0.46$[4] for normal incidence.

The triangular lattice has the same overall characteristics as the square lattice in terms of localized modes at the stopband near the Dirac point. In Fig. 8, we illustrate the electric field localization for the different incident angles. Electric field localization of the order of 10^5 is found inside the stopband.

Different from the square lattice, the electric field in this case is not localized inside the columns but in the space

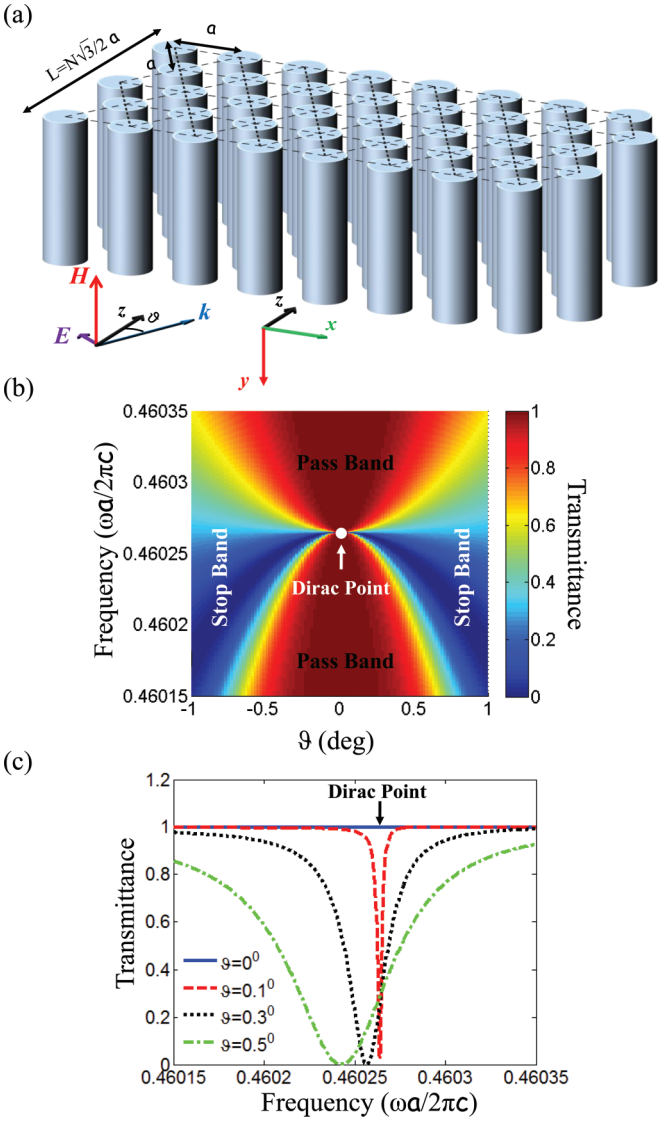

FIG. 7. (Color online) (a) A two-dimensional photonic crystal made of a triangular lattice (lattice constant a) of dielectric columns with radius r and electric permittivity ε. The photonic crystal is finite along the z direction with length $L = N\sqrt{3}/2a$, where N is the number of rows of columns. A plane electromagnetic wave with the magnetic field parallel to the axis of the cylinders (TM polarization) is incident on the structure with its k-vector in the (x, z) plane (in-plane coupling) forming an angle ϑ with respect to the z direction. (b) Transmittance in the (ω, ϑ) plane around the Dirac point numerically calculated by the FMM. The structure's parameters are $N = 5$, $r/a = 0.3$, $\varepsilon = 11.4$. (c) Transmittance vs frequency for different incident angles.

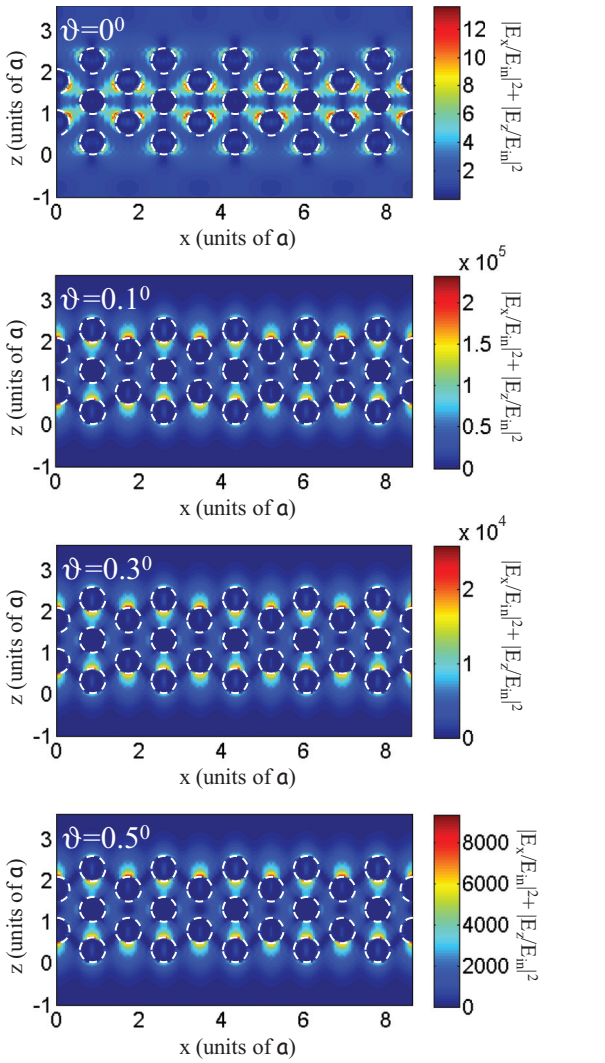

FIG. 8. (Color online) Cross-sectional view of the electric field localization normalized to the incident field for the different incident angles. The dashed circles indicate the position of the columns.

immediately surrounding the columns. This peculiar field localization very near the surface might have useful applications for surface-enhanced processes like Raman scattering from analytes that form a self-assembled monolayer.

III. CONCLUSIONS

We have studied the anomalous localization properties of light near the Dirac point of a two-dimensional photonic crystal and shown how they are related to the GMRs of the structure. These results could have a remarkable influence in many light-matter interaction phenomena in which a high degree of field localization is necessary, such as nonlinear harmonic generation and switching in nanostructures, quantum dot and quantum well emission, Raman scattering, and laser emission. Finally, because of the formal analogy between Maxwell equations in two-dimensional systems under TM polarization and the equations governing sound propagation, we anticipate that similar modes should also exist in the acoustic domain for phononic crystals that admit a Dirac point, such as the one described in Ref. 22, with applications for nonlinear acoustic devices and acoustic sensors.

ACKNOWLEDGMENTS

We acknowledge financial support from DARPA SBIR project W31P4Q-11-C-0109, ARO STTR project W31P4Q-11-C-0098, and ERC grant number 201766.

*Corresponding author: gdaguanno@nanogenesisgroup.com or giuseppe.daguanno@us.army.mil

[1]F. D. M. Haldane and S. Raghu, Phys. Rev. Lett. **100**, 013904 (2008).
[2]S. Raghu and F. D. M. Haldane, Phys. Rev. A **78**, 033834 (2008).
[3]R. A. Sepkhanov, Ya. B. Bazaliy, and C. W. J. Beenakker, Phys. Rev. A **75**, 063813 (2007).
[4]Xiangdong Zhang, Phys. Rev. Lett. **100**, 113903 (2008).
[5]M. Diem, T. Koschny, and C. M. Soukoulis, Physica B **405**, 2990 (2010).
[6]Xueqin Huang, Yun Lai, Zhi Hong Hang, Huihuo Zheng, and C. T. Chan, Nat. Mater. **10**, 582 (2011).
[7]Kazuaki Sakoda, Opt. Express **20**, 9925 (2012).
[8]L. Ferrari and G. Russo, Phys. Rev. B **42**, 7454 (1990).
[9]J. Schliemann, D. Loss, and R. M. Westervelt, Phys. Rev. Lett. **94**, 206801 (2005).
[10]K. S. Novoselov, A. K. Geim, S. V. Morozov, D. Jiang, M. I. Katsnelson, I. V. Grigorieva, S. V. Dubonos, and A. A. Firsov, Nature **438**, 197 (2005).
[11]A. H. Castro Neto, F. Guinea, N. M. R. Peres, K. S. Novoselov, and A. K. Geim, Rev. Mod. Phys. **81**, 109 (2009).
[12]O. Peleg, G. Bartal, B. Freedman, O. Manela, M. Segev, and D. N. Christodoulides, Phys. Rev. Lett. **98**, 103901 (2007)
[13]Li-Gang Wang, Zhi-Guo Wang, Jun-Xiang Zhang, and Shi-Yao Zhu, Opt. Lett. **34**, 1510 (2009).
[14]R. Liu, Q. Cheng, T. Hand, J. J. Mock, T. J. Cui, S. A. Cummer, and D. R. Smith, Phys. Rev. Lett. **100**, 023903 (2008); B. Edwards, A. Alu, M. E. Young, M. Silveirinha, and N. Engheta, *ibid.* **100**, 033903 (2008).
[15]L. Li, J. Opt. Soc. Am. A **13**, 1870 (1996).
[16]S. Gentilini, A. Fratalocchi, L. Angelani, G. Ruocco, and C. Conti, Opt. Lett. **34**, 130 (2009).
[17]See Supplemental Material at http://link.aps.org/supplemental/10.1103/PhysRevB.87.085135 for a movie of the field localization at different incident angles (StopBandModes.wmv).
[18]N. Mattiucci, G. D'Aguanno, M. Scalora, M. J. Bloemer, and C. Sibilia, Opt. Express **17**, 17517 (2009).
[19]D. Pietroy, A. V. Tishchenko, M. Flury, and O. Parriaux, Opt. Express **15**, 9831 (2007); A. E. Miroshnichenko, S. Flach, and Y. S. Kivshar, Rev. Mod. Phys. **82**, 2257 (2010).
[20]G. D'Aguanno N. Mattiucci, M. J. Bloemer, D. de Ceglia, M. A. Vincenti, and A. Alú, J. Opt. Soc. Am. B **28**, 253 (2011); N. Mattiucci, G. D'Aguanno, and M. J. Bloemer, Opt. Lett. **37**, 121 (2012); Opt. Commoun. **285**, 1945 (2012).
[21]See Supplemental Material at http://link.aps.org/supplemental/10.1103/PhysRevB.87.085135 for a movie of the electric field temporal evolution for $\vartheta = 0^\circ$ at the Dirac point and for $\vartheta = 1^\circ$ at the Dirac-point GMR (TemporalEvolution.wmv).
[22]Fengming Liu, Xueqin Huang, and C. T. Chan, Appl. Phys. Lett. **100**, 071911 (2012).